RSC Advances

PAPER

View Article Online
View Journal | View Issue

Cite this: *RSC Adv.*, 2026, **16**, 3443

Novel self-assembled cobalt sulfide nanorods/reduced graphene oxide as an efficient nano-catalyst for dual sensing of 4-nitrophenol

Hanan Alhussain,[a] Arafat Toghan,*[a] N. Roushdy,[b] Sami A. Al-Hussain,[a] Ayman M. Mostafa,[c] Emad M. Masoud,*[d] A. A. M. Farag[e] and Noha A. Elessawy[f]

A sensitive and sustainable electrochemical sensor based on cobalt sulfide nanorods/reduced graphene oxide (CoS-NR/rGO) was fabricated for the detection of 4-nitrophenol (4-NP). rGO derived from recycled plastic waste, served as a conductive and eco-friendly matrix, while CoS-NR were synthesized *via* a simple chemical route using cobalt acetate and thiourea. Transmission electron microscopy (TEM) and scanning electron microscopy (SEM) revealed uniform CoS-NR anchored on thin rGO sheets, forming a high surface area architecture conducive to rapid charge transfer. X-ray diffraction (XRD) confirmed the hexagonal CoS phase and the (002) peak of rGO, whereas Raman spectroscopy identified the D and G bands of rGO and characteristic E_g, F_{12g}, F_{22g}, and A_{1g} vibrational modes for CoS. X-ray photoelectron spectroscopy (XPS) verified the presence of Co^{2+}/Co^{3+}, S^{2-}, and sp^2-hybridized carbon, indicating strong chemical bonding and homogeneous distribution. Electrochemical characterization using cyclic voltammetry (CV) demonstrated enhanced catalytic activity toward 4-NP reduction due to the synergistic effect between CoS and rGO. The sensor achieved high sensitivity (0.118 μA μM^{-1}), a low detection limit (LOD = 2.4 μM), and excellent repeatability over ten cycles. Optimization *via* response surface methodology (RSM) revealed a maximum current response at pH 7 under increased analyte concentration and scan rate. These results establish CoS-NR/rGO as an efficient, reproducible, and environmentally friendly platform for detecting phenolic pollutants.

Received 30th October 2025
Accepted 18th December 2025

DOI: 10.1039/d5ra08356g

rsc.li/rsc-advances

1 Introduction

The plastics industry is one of the largest sectors, seeing significant global expansion, and is widely utilized to manufacture many products that enhance our daily lives. Nonetheless, the discharge of plastic products into landfills and oceans has significantly increased over the past decades, resulting in severe environmental pollution.[1,2] The situation is exacerbated by the involvement of phenolic chemicals in plastic manufacture.[3] Phenolic compounds have the potential to pollute water, causing serious health and environmental damage.[4,5] Because of their toxicity, some are considered hazardous substances or priority pollutants by the US-EPA (U.S. Environmental Protection Agency), including pentachlorophenol, 2-chlorophenol, 2,4,6-trichlorophenol, 2,4-dichlorophenol, 2,4-dimethylphenol, phenol, 2-nitrophenol, 2,4-dinitrophenol, and 4-nitrophenol.[6] Among these phenolic compounds, 4-nitrophenol (4-NP) and its derivatives are extensively used industrially in the production of synthetic dyes, medicines, insecticides, herbicides, pesticides, plastics, and synthetic rubber.[7] Furthermore, because 4-NP is very soluble in aqueous environments, it is present as a contaminant in drinking water and wastewater systems.[8,9] 4-Nitrophenol (4-NP) is recognized by the US-EPA as a hazardous environmental pollutant, and it has been detected in contaminated water at concentrations approaching ~0.4 μM, posing potential risks to water quality and human health.[10] 4-NP is hazardous to microorganisms present in surface water, even at trace levels, and shows greater toxicity than other phenol derivatives.[11] In addition, it is widely known that 4-NP is toxic to humans due to its carcinogenic properties and that even at low levels, it may have negative effects on the liver, kidney, and central nervous system.[12] Therefore, in recent years, considerable attention has been paid to detecting and quantifying 4-NP in aqueous systems. Although the current low detection limit

[a]*Chemistry Department, College of Science, Imam Mohammad Ibn Saud Islamic University (IMSIU), Riyadh 11623, Saudi Arabia. E-mail: aatahmed@imamu.edu.sa*

[b]*Electronics Materials Department, Advanced Technology and New Materials Research Institute, City of Scientific Research and Technological Applications (SRTA-City), New Borg El-Arab City, Alexandria 21934, Egypt*

[c]*Department of Physics, College of Science, Qassim University, P.O. Box 6644, Buraydah Almolaydah 51452, Saudi Arabia*

[d]*Department of Chemistry, Faculty of Science, Islamic University of Madinah, Madinah 42351, Saudi Arabia. E-mail: emad.youssef@iu.edu.sa*

[e]*Thin Film Lab., Department of Physics, Faculty of Education, Ain Shams University, Roxy, Cairo 11711, Egypt*

[f]*Computer-Based Engineering Applications Dept., Informatics Research Institute, City of Scientific Research and Technological Applications (SRTA-City), New Borg El-Arab City, Alexandria 21934, Egypt*

(LOD) of 2.4 μM is higher than the recommended threshold of 0.43 μM for 4-NP in drinking water, the sensor effectively detects 4-NP in low micromolar concentrations. This performance is valuable for preliminary screening and environmental monitoring where rapid, low-cost detection is essential. Additionally, the sensing platform offers potential for further tuning, such as surface modification or compositional adjustments to improve sensitivity and bring the LOD below regulatory thresholds in future developments.

Electrochemical sensors, including voltammetric and amperometric sensors, have been employed extensively in recent decades. When these sensors come into contact with analytes, they detect changes in conductance, voltage, or current that the sensor can measure directly. However, electrode fouling and the requirement for frequent calibration and sample pre-treatment are major disadvantages of electrochemical sensors.[11,13,14]

Designing efficient noble metal-free catalysts, such as metal oxides, carbon-based catalysts, and other composite materials for the detection of harmful pollutants and many other applications, has been a challenge in achieving the same level of activity as noble metals, especially under different environmental conditions, and in fully understanding their catalytic mechanisms. In particular, nanoscale semiconductors have unique properties and have recently found numerous applications, most notably in the assembly of electrochemical sensors.[15,17] The excellent physical-chemical properties, ease of processing, low cost, and large surface area of these materials make them ideal for sensing biomolecules.[16] Because of their remarkable electrical conductivity and redox activity, metal sulfide nanostructures are being utilized more and more to identify different types of contaminants in biological, water, and air samples. Their high efficiency, extreme sensitivity, wide and fast response ranges, and high stability are partly responsible for this growing interest in sensing materials. Among these materials, metal sulfides, such as CoS, ZnS, *etc.*, have been the subject of extensive research interest due to their low toxicity and abundance. They offer enhanced mass transfer, a stronger signal-to-noise ratio, and finer sensitivity, direct band gap, and their properties could be tunable and adaptable in sensor technology.[18–20]

Although researchers are actively working on developing new active materials (noble metal-free catalysts) such as metal oxides, carbon-based catalysts, and other composite materials, challenges still remain in achieving the same activity level as noble metals, especially under different environmental conditions, and in fully understanding their catalytic mechanisms. Interestingly, hybridizing metal chalcogenides, *e.g.* CoS, with conductive materials, such as graphene, certainly overcomes the conductivity limitations of 2D-layered materials and may enhance analyzer sensing. Graphene is the basic unit of graphite and has a unique structure that makes it useful in many applications.[21,22] Graphene oxide (GO) is an essential component for processing many electrochemical sensors, improving their sensitivity in medical and environmental applications.[11,17,19]

4-NP is recognized as a hazardous and persistent pollutant arising from industrial activities such as dye, pesticide, and pharmaceutical production, posing serious environmental and health concerns. Conventional detection methods often suffer from high cost, limited sensitivity, or complicated operation, creating an urgent demand for more efficient monitoring solutions. Recent advances in electrochemical sensing have highlighted the potential of nanostructured composites to enhance detection performance through improved conductivity, surface area, and catalytic activity.

Recent studies have extensively explored the incorporation of conventional nanofillers, such as carbon nanotubes (CNTs) and nanoclays, into polymer-based composites to enhance their mechanical and functional performance, particularly in self-assembled and self-healing systems. Veeramani *et al.*[23] demonstrated that microcapsule-based self-healing composites embedded with CNTs exhibited significantly improved healing efficiency, highlighting the synergistic effect of nanoscale reinforcement on structural recovery. Similarly, Xu *et al.*[24] reported the successful fabrication of nacre-inspired clay/polymer nanocomposites through a self-assembly approach, achieving enhanced toughness and hierarchical organization. Complementing these findings, Naveen *et al.*[25] showed that self-healing microcapsules encapsulating CNTs not only improved mechanical resilience but also enhanced thermal and electrical properties, emphasizing the multifunctional role of CNTs in advanced composites. In addition, Toyama *et al.*[26] illustrated that single-walled CNTs can facilitate catalytic activity when integrated with metallic nanostructures, indicating their versatility beyond mechanical reinforcement. Moreover, Veeramani *et al.*[27] confirmed that the incorporation of polyphenylene ether into carbon fiber/epoxy composites led to a marked increase in fracture toughness, further reinforcing the advantage of using nanofillers to improve composite durability. Collectively, these studies underscore the effectiveness of conventional nanofillers in self-assembly and self-healing matrices to enhance structural and functional properties, providing a strong rationale for exploring hybrid systems such as CoS/graphene oxide to achieve superior mechanical and electrochemical performance.

In this context, the present study introduces a sustainable and innovative approach by utilizing rGO extracted from the recycling of plastic waste as a conductive framework, combined with cobalt sulfide nanorods (CoS-NR) synthesized *via* a simple chemical route. This integration yields a unique CoS-NR/rGO nanocomposite, where well-dispersed CoS nanorods anchored onto rGO sheets provide a high-surface-area and synergistic architecture that enables rapid electron transfer and strong electrocatalytic activity. The novelty lies not only in the environmentally friendly fabrication route but also in achieving a balance between high sensitivity, low LOD, and reproducibility, thereby advancing both sustainable materials science and electrochemical sensor technology. Accordingly, the objective of this work is to design, fabricate, and evaluate an eco-friendly electrochemical sensor based on CoS-nanorods/rGO composite for dual sensing of 4-NP in aqueous environments. The structural, morphological, and chemical features of the fabricated sensor were analyzed and confirmed by XRD, FTIR (Fourier Transform Infrared Spectroscopy), Raman

spectroscopy, XPS, SEM, and TEM. Furthermore, CV was used to explore the electrochemical sensing of CoS-NR/rGO nanocatalyst, such as sensitivity, LOD, and stability. To refine the sensor performance, theoretical investigations including RSM were employed to optimize critical operational parameters such as pH, analyte concentration, and scan rate. Indeed, the results of this work are promising, confirming that coupling CoS nanorods with sustainable material may lead to the design of a potential, reproducible, low-cost, highly sensitive sensor suitable for real-time environmental monitoring of toxic phenolic pollutants.

2 Experimental

2.1 Materials

Cobalt acetate and thiourea powder (Sigma-Aldrich) were thoroughly mixed using a ball mill technique at 800 rpm for 20 min until fine powder was obtained. Then, the collected powder was dissolved in 20 mL of ethanol and allowed to dry at room temperature. The mixture was then heated in an oven at 250 °C for 2 hours to complete the reaction. Finally, fine CoS-nanorod powder was obtained by ball milling again (under the same initial conditions). Scheme 1 displays the steps of fabricating CoS-nanorods. To prepare rGO powder, waste polyethylene terephthalate (PET) drinking water bottles were shredded and then subjected to pyrolysis at 800 °C for 1 hour.[28,29]

2.2 Characterization techniques

Several analytical methods were used to characterize the produced powder (CoS-NR or rGO). Using a JEOL JSM-6360LA (Japan) scanning electron microscope (SEM), the morphological features were examined. A JEOL JEM2100 plus (Japan) was used for transmission electron microscopy (TEM), which provided additional information on the morphology. Powder-XRD (Shimadzu-7000, Japan), FTIR (Nicolet IS10 spectrophotometer), Raman spectroscopy (514.5 nm laser beam, SENTERRA model, Bruker-Germany), and XPS (PerkinElmer Phi 5300 ESCA) were employed to verify and analyze the structure and composition of the fabricated materials.

2.3 Electrode preparation

The electrode ink for the blank sample was prepared by mixing 10 mg of CoS nanorods (CoS-NR), 10 mg of polyvinylidene fluoride (PVDF), and 2 mL of *N*,*N*-dimethylformamide (DMF).

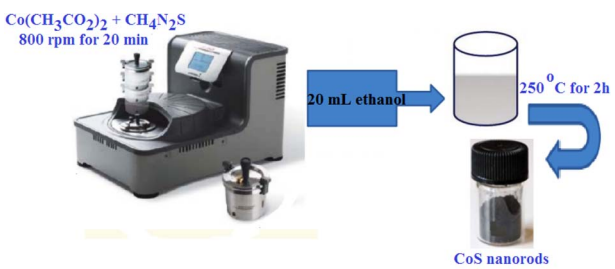

Scheme 1 Reaction pathway for the synthesis of CoS-nanorods.

For the CoS-NR/reduced graphene oxide (rGO) composite, a weight ratio of 1 : 1 (50 wt% rGO) was employed, combining 10 mg of composite powder with 10 mg of PVDF and 2 mL of DMF. This maximum rGO loading was chosen to balance high conductivity and surface area while preventing rGO aggregation, which can reduce electrode uniformity. The mixture was ultrasonicated for 15 minutes to achieve a homogeneous dispersion. Finally, 10 μL of the uniform ink was drop-cast onto a glassy carbon electrode (GCE, 0.126 cm^2) and dried for 2 hours to form a stable and reproducible electrode coating.

2.4 Electrochemical measurements

A potentiostat (Autolab 87070, Metrohm) in a two-electrode configuration was used to perform all electrochemical tests. In this arrangement, the CoS-NR or CoS-NR/rGO composite coated electrodes functioned as the working electrode, while a platinum (Pt) wire served as the counter electrode. Repeated CV scans were performed in 0.1 M PBS (phosphate buffer solution), which serves as a supportive electrolyte at pH 7, at scan rates ranging from 10 to −100 mV s^{-1}.

S/N = 3 was used to quantify the signal for the measurement and the noise level in order to estimate limits of detection (LOD) from single measurements. From the calibration curve regression line, analytically valid LODs were computed by dividing the regression line's slope by three times the regression line's standard deviation.

To assess the reusability and operational stability of the CoS-NR/rGO-modified electrode for 4-nitrophenol detection, repeated electrochemical measurements were carried out over five successive cycles. The electrode maintained approximately 92% of its initial current response, indicating reliable performance upon repeated use. In addition, after being stored under ambient conditions for two weeks, the electrode exhibited only slight variation in its response, confirming its structural and functional stability over time. These findings support the electrode's suitability for sustained sensing operations.

The sensor's selectivity was further evaluated by introducing common interfering species such as nitrite, glucose, urea, and ascorbic acid at relevant concentrations. These compounds produced negligible interference in the current response, affirming the sensor's high specificity toward 4-nitrophenol. For long-term stability, the modified electrode was monitored over a 21 day period. It retained over 93% of its initial electrochemical response, underscoring its durability. Together, these results demonstrate that the CoS-NR/rGO-based sensor is both selective and stable, making it a promising candidate for reliable, real-world environmental monitoring applications.

3 Results and discussion

3.1 Surface investigations

The microstructures and morphological characteristics of the synthesized samples (CoS-NR and rG) were explored by TEM and SEM. As seen in Fig. 1a, the SEM image of the designed cobalt sulfide confirmed the formation of a homogenous rod-shaped structure. These clusters have an uneven arrangement,

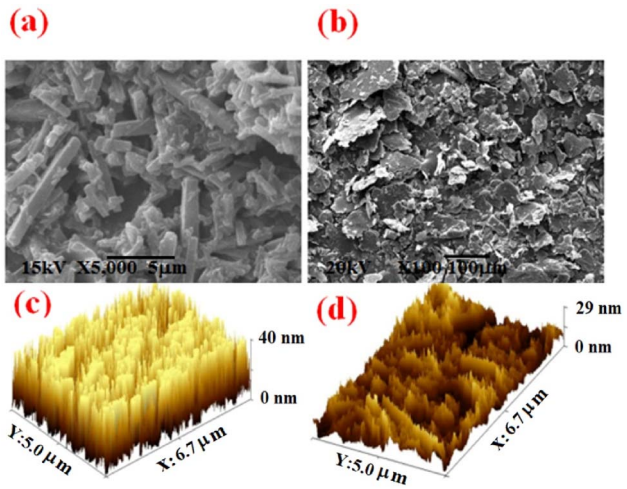

Fig. 1 SEM micrographs of: top-view of (a) CoS-NR, (b) rGO , (c) height profile provided from 2D-images of CoS-NR , and rGO (d).

showing an overall uneven structure. While the rGO particles appear sheet-like and have distinct boundaries, the clumping remains evident as shown in Fig. 1b. Undoubtedly, this distinct morphological structure of CoS-NR and rGO is reflected in their functional properties and performance.[30] Additionally, the corresponding 2D SEM surface topography and their extracted height profiles for both CoS-NR and rGO were analyzed to provide a clearer representation of the surface morphology, as illustrated in Fig. 1c and d, respectively. These 2D images offer a broader spatial perspective of the nanostructure distribution, enabling a more reliable interpretation than the line-scan height profiles alone. The CoS-NR film exhibits a densely packed network of vertically oriented nanorods with noticeable variations in height, reflecting the intrinsic anisotropy of the growth process. In contrast, the rGO sample displays a wrinkled, sheet-like architecture, consistent with the layered nature of graphene-based materials.

The combined visualization of the 2D topography and height profiles highlights the presence of surface irregularities, localized agglomeration, and structural heterogeneity that cannot be fully resolved from a single front-view SEM micrograph. To quantitatively assess these morphological variations, the average roughness and root mean square (RMS) roughness were calculated using ImageJ, allowing a more accurate comparison of the surface complexity of both materials. These roughness parameters provide valuable insight into the nanoscale texture, which is directly linked to their electrochemical activity, interfacial behavior, and potential sensing performance.[22]

Fig. 2 showcases TEM micrographs of the prepared CoS-NR, rGO, and CoS-NR/rGO nanocomposite, delivering an in-depth examination of its nanostructure. Interestingly, in complete agreement with the results of SEM, the TEM image of cobalt sulfide (Fig. 2a) illustrates the formation of rod-shaped structures with a high degree of aggregation of CoS nanoparticles. The low magnification image (Fig. 2b) shows rGO as an irregular transparent layer with ripples appearing at the edges. In the CoS-NR/rGO composite (Fig. 2c), the CoS-NR appear as dark clusters partially distributed across the rGO sheets rather than being perfectly uniform. This distribution reflects the intrinsic tendency of rGO sheets to restack due to van der Waals interactions and the aggregation of CoS-NR driven by surface energy. To address this, the composite was ultrasonicated for 15 minutes, which sufficiently exfoliates rGO sheets and disperses the nanorods without causing significant structural fragmentation. Extending sonication beyond this duration was avoided because prolonged energy input can break the CoS nanorods into smaller fragments and induce partial restacking of rGO, ultimately reducing effective surface area and electron transport pathways. The observed microstructure therefore represents an optimized compromise: CoS-NR are adequately distributed to maintain high surface contact with rGO, ensuring effective charge transfer and electrocatalytic activity, while preserving the structural integrity of both components. This dispersion is sufficient for the intended electrochemical applications, balancing material stability and functional performance.

3.2 Structural and molecular characterizations

The XRD pattern of CoS-NR (Fig. 3a) clearly displays reflections characteristic of the hexagonal CoS phase (JCPDS #03-065-3418), with peaks at $2\theta = 35.50°$, $42.35°$, $54.82°$, and $61.53°$, corresponding to the (101), (102), (110), and (103) planes, respectively. The sharp and well-defined peaks confirm the formation of the intended phase and indicate a significant degree of long-range order.[31] However, the moderate intensity and slight broadening of the peaks suggest the presence of nanoscale crystalline domains and partial structural disorder. Using the Scherrer equation ($K = 0.9$, $\lambda = 1.5406$ Å) applied to

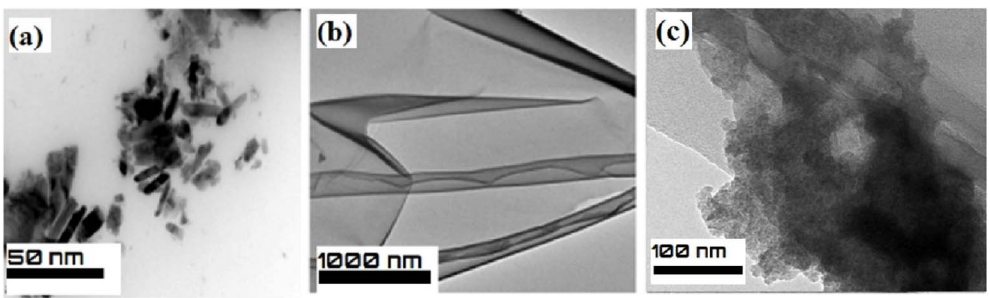

Fig. 2 TEM micrograph for (a) CoS-NR, (b) rGO, and (c) CoS-NR/rGO.

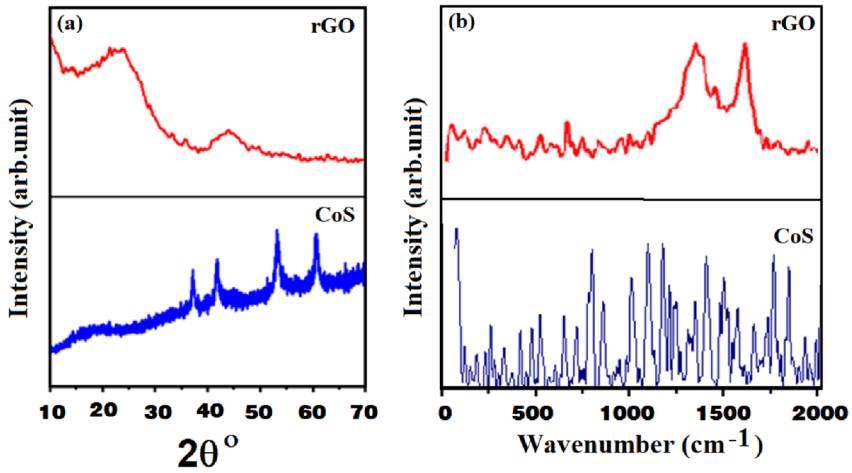

Fig. 3 (a) XRD, and (b) Raman patterns for CoS-NR and rGO.

the most intense peak with a representative FWHM, the average crystallite size is estimated to be approximately 32.9 nm. The degree of crystalline peak areas relative to the total diffracted intensity across the scanned 2θ range is about 80%. These observations indicate that the CoS nanorods are composed of well-ordered but nanoscale domains, where finite crystallite size contributes to the peak broadening and minor amorphous content accounts for the residual disordered fraction.

The combination of nanoscale crystallites, partial crystallinity, and subtle peak broadening has important implications for the material's properties. The nanoscale dimensions and high surface-to-volume ratio of the crystalline domains enhance surface reactivity, which is advantageous for electrochemical applications, sensing, and catalysis. Meanwhile, the presence of minor disorder or amorphous regions may introduce lattice strain and defect sites that can influence charge transport and optical behavior. The coherence length estimated from the Scherrer analysis represents the size of diffracting domains rather than the full length of the nanorods, highlighting the anisotropic nature of the rods. Overall, the structural characteristics revealed by XRD, phase purity, nanoscale crystallite size, and partial crystallinity provide a strong foundation for correlating the CoS-NR morphology with functional performance, while suggesting that further optimization of grain boundaries and strain could enhance electronic and catalytic properties.

In contrast, the XRD spectrum of rGO displays a broad and low-intensity peak centered around 24°, corresponding to the (002) plane of stacked graphene layers.[32] This pronounced broadening, along with a weaker peak near 43.97° (assigned to the (100) plane, indicates a highly disordered and exfoliated nanostructure with minimal long-range order. The diffuse nature of these peaks is characteristic of reduced graphene oxide, where incomplete restacking and residual oxygen functional groups disrupt crystallinity. Such features are typical of nanostructured carbon materials, where reduced domain size and structural defects enhance surface area and facilitate charge transport, making rGO suitable for applications in energy storage and catalysis.

In the Raman spectra (Fig. 3b) of CoS-NR, the modes E_g, F_{12g}, F_{22g}, and A_{1g} indicate four peaks positioned at 455,505, 595, and 660 cm^{-1}. These four characteristic peaks corresponding to the function groups can be repeated around the other wavenumbers 7000, 1000, 1500, 1700, 2000, and 2250 cm^{-1}.[33] However, the rGO's Raman spectra display the two characteristic peaks of graphitic carbon materials: The D band at 1338 cm^{-1} is due to defects in the rGO layer, and the G band at 1603 cm^{-1} is from the sp^2 hybrid system.[32] It is worth noting that the results of SEM, TEM, XRD, and Raman spectroscopy support and agree well with each other to confirm the formation of a hexagonal rod-shaped structure of the CoS nanoparticles.

Fig. 4 displays the FTIR spectra of pristine CoS-NR, CoS-NR anchored on rGO, and the CoS-NR/rGO composite after interaction with 4-NP, allowing a clear comparison of the surface functionalities and the strength of hydrogen-bonding interactions among the three systems. In spectrum (a), the CoS-NR show characteristic bands corresponding to O–H stretching in adsorbed moisture around the broad region of 3300–3400 cm^{-1}, along with distinct metal–sulfur vibrational modes appearing in the fingerprint region below 700 cm^{-1}. When CoS is integrated with rGO (spectrum b), the O–H band becomes noticeably broader and more intense, indicating the establishment of stronger hydrogen bonding between the oxygenated groups of rGO and the surface of the CoS-NR. Additional vibrations assigned to C=O and C–O stretching of rGO become evident near 1710–1600 cm^{-1} and 1200–1050 cm^{-1}, confirming successful hybridization between the two components.

Upon exposure of the CoS-NR/rGO composite to 4-NP (spectrum c), further spectral shifts and intensity changes are observed. The O–H band exhibits a clear red-shift and enhanced broadening, reflecting strong H-bonding interactions between the phenolic –OH group of 4-NP and the oxygenated sites on rGO, as well as potential coupling with surface Co sites. The bands appearing around 1520–1340 cm^{-1} correspond to the asymmetric and symmetric stretching modes of the $-NO_2$ group, confirming the successful adsorption of 4-NP onto the composite surface. The extent of band shifting in this region, compared to spectra (a), and (b), further supports the formation

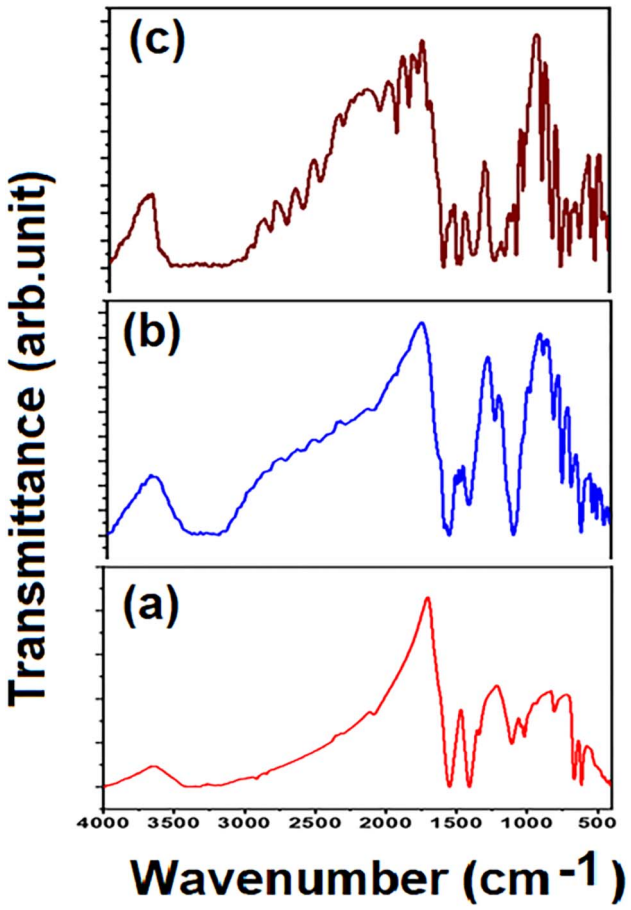

Fig. 4 FTIR of: (a) pristine CoS-NR, (b) CoS-NR/rGO, and (c) CoS-NR/rGO in the presence of 4-NP.

of a stable interaction, likely through hydrogen bonding and π–π stacking with rGO. Overall, the progressive broadening, shifting, and emergence of specific vibrational modes across the three spectra provide strong evidence that the CoS-NR/rGO composite offers enhanced interaction sites, enabling stronger and more specific H-bonding interactions with 4-NP compared to the standalone CoS-NR.

To identify the composition of the designed CoS-NR/rGO nanocomposite, XPS has been performed. Fig. 5a shows the full scan spectrum of CoS-NR/rGO in which four significant peaks can be seen at the binding energies (BEs) of 172, 285, 534, and 793 eV, which correspond to S 2p, C 1s, O 1s, and Co 2p, respectively. The XP spectra of C 1s of rGO were fitted into four characteristic peaks at 289.5, 287, 285.3, and 284.5 eV which correspond to the carboxylic, C=O, epoxide, and sp^2 carbon in the aromatic rings, respectively (Fig. 5b).[34] As shown in Fig. 5c, the Co 2p spectra indicate a match with the BEs at 781 and 796.6 eV for the $2p_{3/2}$ and $2p_{1/2}$ of Co^{3+}, respectively. However, the BEs at 784.3 and 799 eV correspond to the $2p_{3/2}$ and $2p_{1/2}$ of Co^{2+}, respectively.[35] In Fig. 5d, the XPS spectrum of S 2p was divided into two main peaks centered at 161.4 and 162.2 eV, referred to as S $2p_{3/2}$ and S $2p_{1/2}$ peaks of S-metal, respectively.[36] Strictly speaking, the regular partial distribution of elements can definitely modify the physicochemical, catalytic, electrochemical, and electrical properties of CoS-Nr/rGO composite.[37] The incorporation of rGO certainly enhances the electrical properties of CoS nanomaterials and thus improves the electrochemical response of the sensor.[38,39]

3.3 Electrochemical sensing of 4-NP

Fig. 6 shows the comparison of electrocatalytic redox of 4-NP on bare GCE, pristine CoS-NR, and CoS-NR/rGO composite in a potential window of −1.0 to +1.0 V. The bare GCE does not show any peaks, indicating no or poor electron transfer kinetics due to its limited active sites and weak catalytic activity.[40] In contrast, the CoS-NR electrode demonstrates a significantly enhanced current response, attributed to the increased number of active sites provided by the nanostructured CoS. Interestingly, the most pronounced improvement is observed with the CoS-NR/rGO composite, where the peak current is further enlarged. This enhancement cannot be solely attributed to the individual contributions of rGO or CoS-NR but rather to their synergistic interaction, which facilitates faster electron transfer and improved catalytic efficiency.

The superior performance of the CoS-NR/rGO electrode stems from the synergistic effects between CoS-NR and rGO. The hydrogen bonding interaction between the functional groups of rGO and the OH group of 4-NP enhances the adsorption of 4-NP onto the electrode surface, thereby increasing the electrochemical sensing.[40] Additionally, the heterogeneous structure of the composite prevents nanoparticle aggregation, ensuring a high specific surface area and improved conductivity. This structural advantage is absent in the individual components, as rGO alone lacks sufficient catalytic activity, while CoS-NR suffers from limited conductivity and particle aggregation. The composite's ability to combine the catalytic properties of CoS-NR with the conductive and adsorptive capabilities of rGO results in a more efficient reduction process, as evidenced by the positively shifted reduction peaks and higher current response.

The CoS-NR/rGO composite outperforms its individual components due to its integrated physicochemical properties. The reversible redox processes observed at high potentials, attributed to the conversion between 4-hydroxyaminophenol and 4-nitrosophenol, highlight the composite's catalytic versatility.[41,42] Moreover, the irreversible reduction peak at low potentials (at −0.35 V), corresponding to the reduction of 4-NP to hydroxylaminophenol, underscores the composite's ability to drive multiple reaction pathways. These features are absent or less pronounced in the individual CoS-NR and rGO electrodes, demonstrating the composite's superior catalytic performance. The enhanced current response, improved peak potential shifts, and prevention of nanoparticle aggregation collectively confirm that the CoS-NR/rGO composite is a more effective electrocatalyst for 4-NP reduction than its standalone counterparts.

Fig. 7a represents the response of the CoS-NR/rGO composite electrode to a change in 4-NP concentration from 0 to 4 mM at room conditions. It was observed that the reduction current responses are increased from lower to higher concentration, which further confirmed the excellent

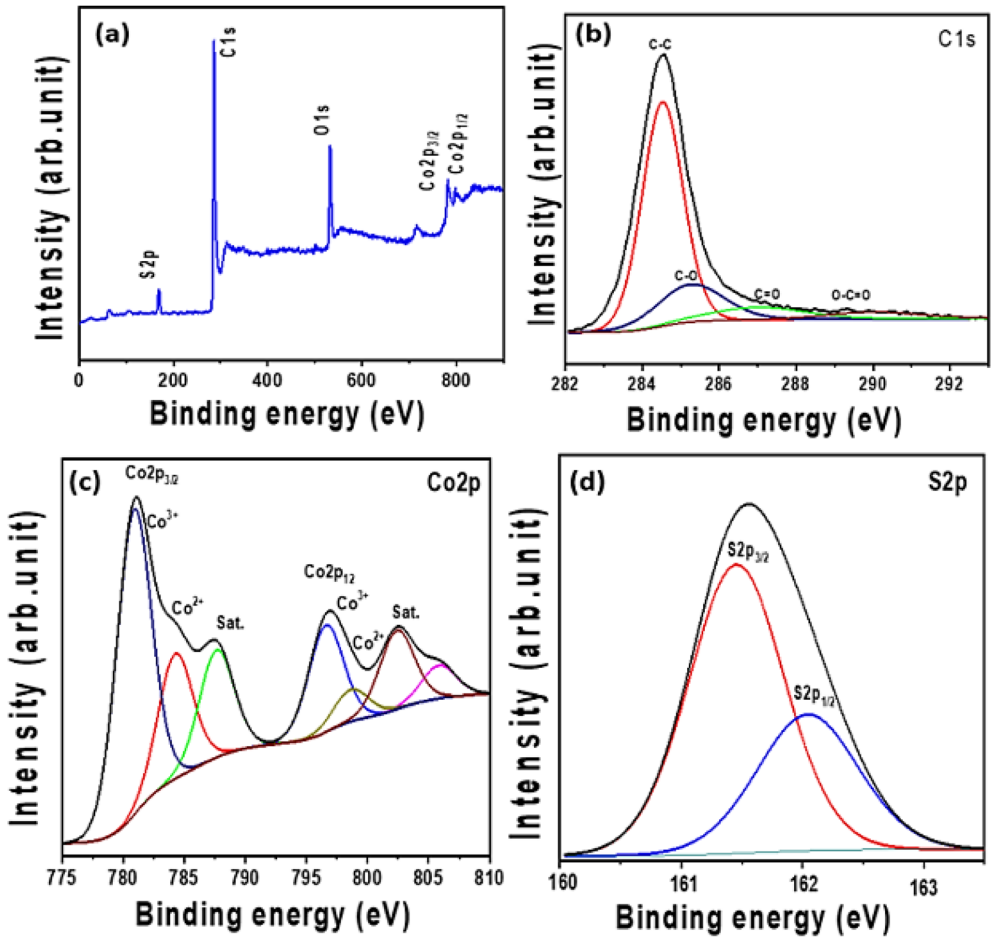

Fig. 5 XPS spectra of CoS-NR/rGO nanocomposite: (a) full survey scan, (b) C 1s, (c) Co 2p, and (d) S 2p.

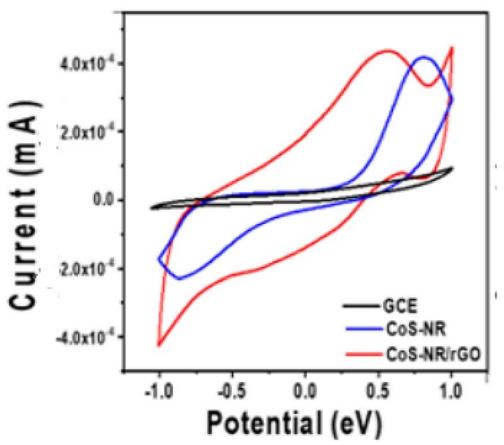

Fig. 6 Comparison of electrocatalytic redox of 4-NP in 0.1 M PBS on surfaces of: bare GCE, pristine CoS-NR, and CoS-NR/rGO composite.

electrocatalytic reduction activity of CoS-NR/rGO towards 4-NP. Moreover, the increased maximum current indicates the superior sensitivity of the CoS-NR/rGO composite towards the accurate detection of 4-NP levels.[38,39] The correlation of the reduction peak currents at −0.35 V and 4-NP concentrations (0–4 mM) is shown in Fig. 6b. The graph shows a linear dependence with a correlation coefficient (R^2) of 0.965, which, although not perfect, is within the acceptable range. Importantly, the cathodic peak current increased proportionally with the concentration of 4-NP up to 3 mM, indicating a consistent electrochemical response. This behavior is attributed to the adsorption of 4-NP molecules onto the CoS-NR/rGO surface, followed by electron transfer during reduction. The observed decline in peak current beyond 3 mM is likely due to saturation at the active sites, a well-documented phenomenon in surface-controlled electrochemical systems, which supports the assertion that the electrode operates through an adsorption-driven catalytic mechanism.

We agree that the current at 0 mM should not be included in the calibration range, as it does not represent an analyte signal. In our revised manuscript, we have redefined the linear range to begin at the lowest detectable concentration that yields a valid analytical signal above the background—consistent with good analytical practice. The LOD was estimated using the standard 3σ/slope method and calculated to be 2.4 μM, with a corresponding sensitivity of 0.118 μA μM^{-1}. These values reflect the sensor's performance at a signal-to-noise ratio of 3, and the LOD unit has now been corrected to μM throughout the manuscript for accuracy and consistency.

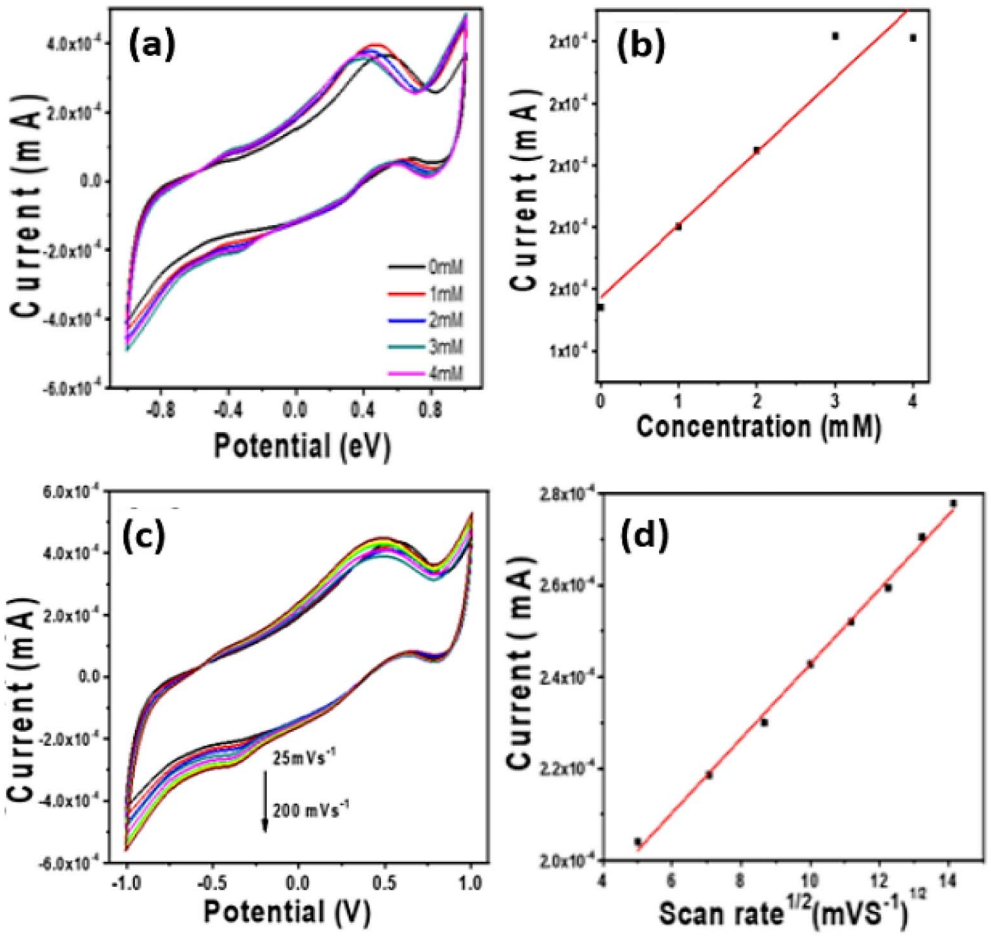

Fig. 7 (a) CVs for CoS-NR/rGO at various 4-NP concentrations (0–4 mM), (b) dependence of reduction peak currents at −0.35 V on 4-NP concentrations, (c) CV curves for CoS-NR/rGO sensor at different scan rates, and (d) linear fitting of reduction peak currents at −0.35 V to $\nu^{1/2}$.

While we recognize that our sensor does not offer the lowest LOD reported in the literature, it presents significant strengths, including ease of synthesis, structural stability, good reproducibility, and a clear electrochemical response across the target concentration range. The CoS-NR/rGO composite demonstrates strong electrocatalytic activity for phenolic compound detection, and the behavior we observed is consistent with known electrochemical mechanisms involving adsorption-limited reduction at modified electrodes. Thus, we respectfully submit that our work offers valuable insights into the design and application of nanostructured electrochemical sensors and merits consideration for publication.

To understand the kinetics of the electrochemical sensing process, the impact of scanning speed on the 4-NP detection performance was also investigated. The CV curves of the CoS-NR/rGO sensor electrode under scanning rate ranging between 25–200 mVs^{-1} at pH = 7 and 4-NP (3 mM) are shown in Fig. 7c. It was observed that, as the scanning speed increases, the reduction peak current gradually rises and that the peaks are moved toward higher negative potentials, indicating that the reduction process at the electrode surface is diffusion controlled. Additionally, the reduction peak current is linearly proportional to $\nu^{1/2}$ (square root of scan rate) of the scanning rate (Fig. 7d) with a correlation coefficient (R^2) of 0.996, which again confirms the occurrence of a diffusion-controlled electron transfer process on the CoS-NR/rGO surface.[42]

The electrocatalytic activity of the CoS-NR/rGO electrode toward 4-NP was strongly influenced by the pH of the electrolyte solution. CV measurements were conducted over a pH range of 5 to 9 (Fig. 8a), revealing a distinct dependence of the peak reduction current on the proton concentration. As the pH increased from 5 to 7, the reduction peak current increased markedly, reaching a maximum at pH 7, indicating that near-neutral conditions favor optimal electron transfer and efficient catalytic activity. This enhancement can be attributed to the balanced availability of protons, which are required for the electrochemical reduction of the nitro group in 4-NP, without causing excessive surface saturation that would block active sites. Beyond pH 7, the peak current gradually decreased, reflecting a decline in electrocatalytic efficiency. At higher pH values, the lower proton concentration reduces the availability of protons for the reduction reaction, while increased hydroxide ion concentration may compete with 4-NP adsorption on the electrode surface, hindering electron transfer.[43,44] These observations highlight the crucial role of electrolyte pH in tuning the electrocatalytic performance of CoS-NR/rGO composites and

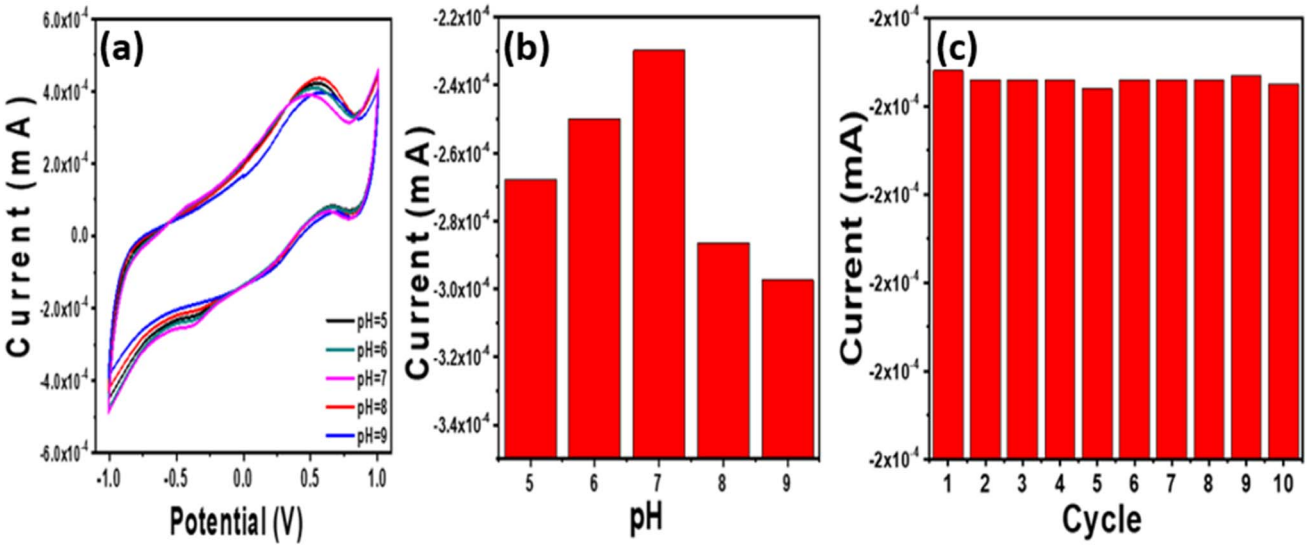

Fig. 8 (a) CVs of CoS-NR/rGO at different pH values in presence of 4 mM 4-NP, (b) dependence of reduction peak currents at −0.35 V on pH, (c) effect of repeated cycling (10 cycles) of 4 mM of 4-NP at CoS-NR/rGO electrode.

align with previously reported trends in 4-NP electroreduction using similar nanostructured electrodes.[43,44]

In acidic conditions (pH < 7), the abundance of hydronium ions in the solution competes with 4-NP molecules for the active sites on the CoS-NR/rGO surface. This competition reduces the number of active interactions between 4-NP and the electrode, thereby suppressing the reduction reaction. The electrode surface becomes saturated with protons, which not only blocks access to catalytic sites but may also interfere with the reduction of the nitro group in 4-NP, leading to decreased current response.[43,44]

At alkaline pH values (pH > 7), although proton availability becomes less of a limiting factor, deprotonation of 4-NP increases the electron density on the $-NO_2$ group. This negatively charged species experiences electrostatic repulsion from the also negatively charged CoS-NR/rGO surface, which in turn hinders effective electron transfer. This repulsion slows down the reduction of kinetics, resulting in a decrease in current. Based on these observations, a pH of 7.0 was selected as the optimal condition for subsequent electrochemical sensing experiments (see Fig. 8b).

To assess the electrochemical stability of the CoS-NR/rGO-modified electrode, repeated CV scans were performed in the presence of 4-NP. As presented in Fig. 8c, the reduction peak current remained nearly unchanged after ten successive voltage cycles, indicating that the sensor maintains a stable electrocatalytic response over repeated measurements. This behavior confirms the electrode's excellent operational durability, which is crucial for real-world applications where consistent performance over time is required. The ability to retain its sensing capability after continuous cycling highlights the robustness of the CoS-NR/rGO composite film and the strong adhesion of the active material to the electrode surface.

In addition to stability, the reproducibility of the sensor fabrication process was evaluated by preparing three separate CoS-NR/rGO electrodes using the same synthesis protocol described in Section 2.3. These electrodes were tested under identical conditions to determine variations in their electrochemical responses. The comparison revealed minimal differences in the recorded peak currents for 4-NP reduction across the three electrodes. The calculated RSD (relative standard deviation) was only 1.184%, which demonstrates high reproducibility in the electrode preparation method. Such low variability confirms that the fabrication process is reliable and consistent, ensuring that the sensor performance can be reproduced across multiple batches without significant deviation.[45,46]

3.4 Electrochemical sensing mechanism

The electrochemical reduction mechanism of 4-NP has been widely investigated and documented in the literature.[47–49] Most studies agree that the process involves a stepwise reduction of the nitro group through intermediate species such as nitrosophenol and hydroxylaminophenol, often with the participation of multiple electrons and protons. For instance, Deng *et al.*[48] reported two redox peaks attributed to the transformation between 4-hydroxylaminophenol and 4-nitrosophenol on a modified electrode, while Luo *et al.*[49] observed a well-defined reduction signal on carbon nanotube-modified electrodes, confirming a multi-electron transfer process. Similarly, Hu *et al.*[50] described a four-electron, four-proton irreversible reduction of 4-NP to hydroxylaminophenol on a chemically modified electrode.

As illustrated in Fig. 9, the CoS-NR/rGO-modified electrode demonstrates distinct redox behavior corresponding to the electrochemical reduction of 4-NP. The CV profile reveals both reversible and irreversible processes: the reversible redox peaks arise from the interconversion between nitrosophenol and hydroxylaminophenol, while a pronounced irreversible peak at

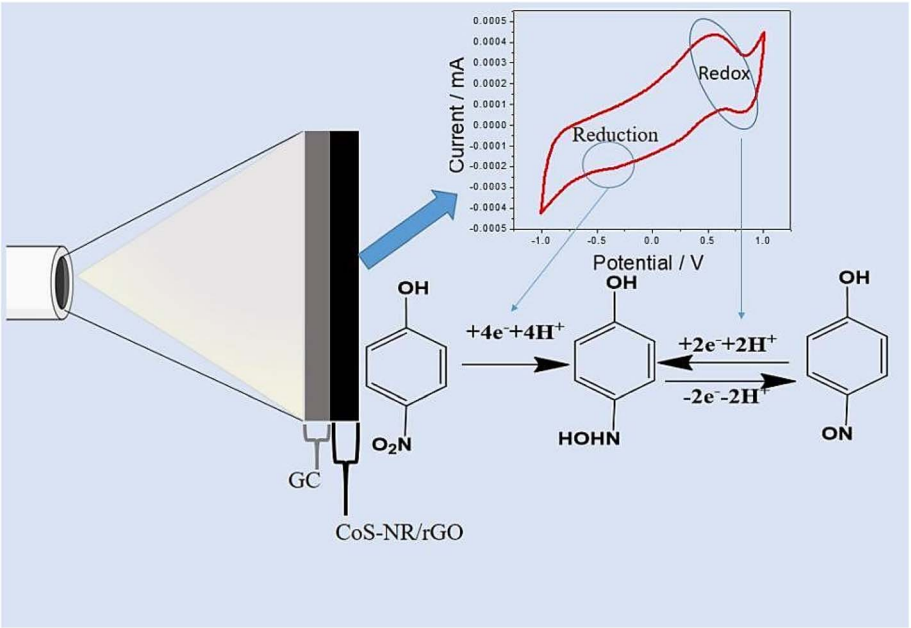

Fig. 9 The electrochemical mechanism of 4-NP on CoS-NR/rGO surface.

a lower potential corresponds to the direct reduction of the nitro group to hydroxylamine, proceeding *via* a concerted four-electron, four-proton transfer. Although this mechanistic pathway is consistent with prior studies,[48–50] its inclusion here underscores the specific electrocatalytic advantages of the CoS-NR/rGO composite. The synergistic combination of CoS-NR and rGO provides a high density of active sites, including surface defects and oxygen-containing functional groups, which enhance the adsorption of 4-NP molecules. These features facilitate rapid electron transfer and reduce overpotential, leading to increased peak currents and improved sensing efficiency. Additionally, the conductive rGO network ensures efficient charge transport, while the nanoscale CoS structures offer localized catalytic centers, collectively amplifying the electrocatalytic response. This discussion highlights how the unique structural and chemical characteristics of the composite optimize the reduction process within a well-established electrochemical framework.

3.5 Optimization of detecting parameters

The electrocatalytic efficiency of CoS-NR/rGO towards 4-NP is expected to be affected by several factors, including electrolyte pH, analyte concentration, and scanning speed. Those parameters were optimized by utilizing the response surface methodology model (RSM) to create a link between the components and the related attributes. The chosen matrix for the response surface methodology, following 17 trials, adhered to the Box–Behnken design,[47] whereas three variables were employed to assess the electrocatalytic activity: A (the electrolyte pH value), B (4-NP concentration, mM), and C (scan rate, mVs^{-1}), at 3-levels (−1, 0, and 1). Design-Expert software (13.0.9.0, STAT-EASE, INC) was used to do this.

Indeed, the coded equation serves as an aid to comparing factor coefficients to estimate the relative effect of each factor on the result variable. Assume that quadratic dependence represents the statistical correlation between variables A, B, and C, and the reduction current (r_c). So, the following equations, which can be used to predict the response to certain levels of each factor, are:

$$\begin{aligned} Y_{r_c} = {} & -0.001867 + (1.9250000000001 \times 10^{-6})\, A \\ & + (5.1475 \times 10^{-5})\, B + (1.455 \times 10^{-5})\, C \\ & + (3.64 \times 10^{-5})\, \mathrm{AB} + (1.725 \times 10^{-5})\, \mathrm{AC} \\ & - (1.095 \times 10^{-5})\, \mathrm{BC} - (8.515 \times 10^{-5})\, A^2 \\ & - (3.29 \times 10^{-5})\, B^2 - (1.165 \times 10^{-5})\, C^2 \end{aligned} \quad (1)$$

Fig. 10 depicts the results of the Box–Behnken design analysis in contour plots that show some interaction between the current reduction and the tested variables. It was observed that as the scan rate and 4-NP concentration increased, the electrocatalytic activity of CoS-NR/rGO towards 4-NP increased and reached a maximum at an electrolyte pH equals 7.

The ANOVA method was employed to evaluate the statistical significance of the quadratic response surface model. The R^2 coefficient is close to one (0.9860) for the quadratic model, indicating a good fit with the experimental data. By examining the data in Table 1, it appears that the chosen quadratic model is statistically significant because the obtained p-values are less than 0.05. The low P value also indicated that the variables had a drastic influence on the electrocatalytic activity of CoS-NR/rGO. Following this investigation, the optimal conditions appeared to involve utilizing the variables at their maximum values, resulting in a reduction in current at low potential values of approximately 0.0002 mA.

Although the CoS/rGO/GCE exhibits a LOD of 2.4 μM with a linear range of 10–100 μM, which appears higher and narrower than several sensors reported in the literature, its performance remains valid within practical applications

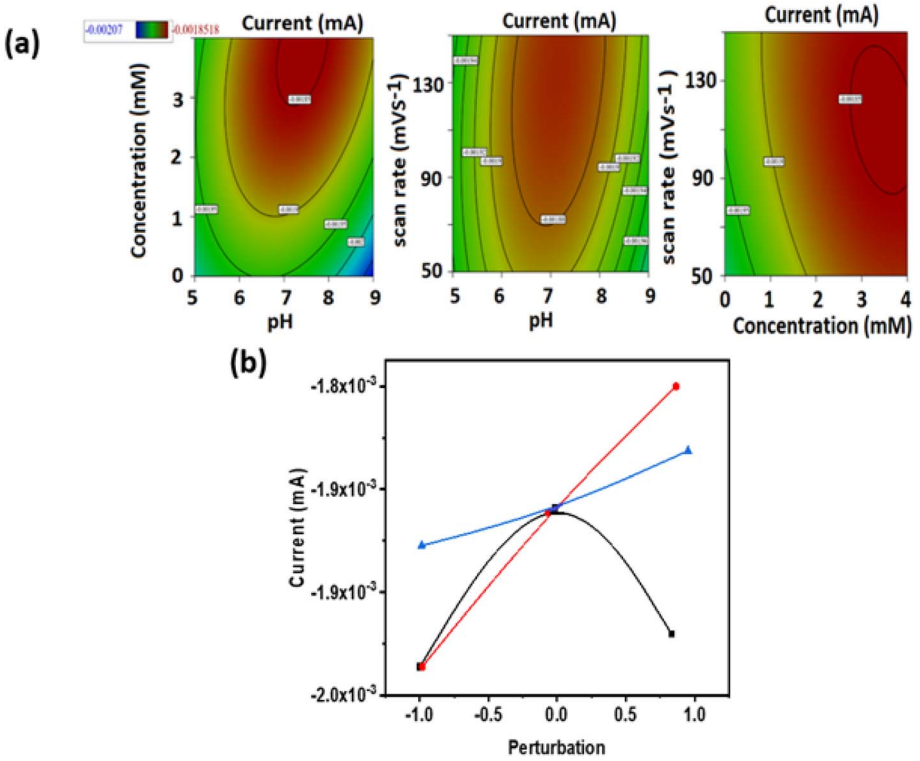

Fig. 10 (a) Contour plots of the electrocatalytic activity of CoS-NR/rGO towards 4-NP *vs.* assigned variables, (b) plot of current *vs.* perturbation *vs.* current under the effect of the assigned variables on the electrocatalytic activity at pH = 7, and scan rate = 100 mV s^{-1}.

involving higher concentrations of 4-NP, especially in industrial and environmental contexts. For instance, AgPd@UiO-66-NH2/GCE[51] and Ag NPs/GCE[52] demonstrated extremely low LODS of 0.032 μM and 0.015 μM, respectively, but their synthesis involves complex procedures and noble metals, which may hinder large-scale implementation. Similarly, sensors such as GO/GCE,[53] OMCs/GCE,[54] and MIP/ZnO-MWNTs-CTS/ITO[55] achieved impressive sensitivity with LODs of 0.02, 0.1, and 0.009 μM, respectively, but often required molecular imprinting, sol–gel processes, or multi-step functionalization. While MWCNTs-MnO_2/GCE,[56] Sm_2O_3 NPs@f-CNFs/SPCE,[57] NiONPs-NH3MPF6/CPE,[58] and PCZ@N-GE/GCE[59] demonstrated LODs ranging from

Table 1 ANOVA analysis for the quadratic model

Source	Sum of squares	df	Mean square	*F*-value	*p*-value	
Model	6.772×10^{-8}	9	7.525×10^{-9}	54.97	<0.0001	Significant
A-pH	2.965×10^{-11}	1	2.965×10^{-11}	0.2166	0.6558	
B-4-NP conc.	2.120×10^{-8}	1	2.120×10^{-8}	154.86	<0.0001	
C-scan rate	1.694×10^{-9}	1	1.694×10^{-9}	12.37	0.0098	
AB	5.300×10^{-9}	1	5.300×10^{-9}	38.72	0.0004	
AC	1.190×10^{-9}	1	1.190×10^{-9}	8.70	0.0214	
BC	4.796×10^{-10}	1	4.796×10^{-10}	3.50	0.1034	
A^2	3.053×10^{-8}	1	3.053×10^{-8}	223.03	<0.0001	
B^2	4.558×10^{-9}	1	4.558×10^{-9}	33.30	0.0007	
C^2	5.715×10^{-10}	1	5.715×10^{-10}	4.17	0.0803	
Residual	9.582×10^{-10}	7	1.369×10^{-10}			
Lack of fit	9.562×10^{-10}	3	3.187×10^{-10}	637.45	<0.0001	Significant
Pure error	2.000×10^{-12}	4	5.000×10^{-13}			
Cor total	6.868×10^{-8}	16				
Std. Dev	$1.1699633693899 \times 10^{-5}$					
Mean	−0.0019					
C.V. %	0.6068					
R^2	0.9860					
Adjusted R^2	0.9681					
Predicted	0.7772					

0.00261 to 0.64 μM, their fabrication involves costly or less accessible precursors and intricate synthetic control. In contrast, the CoS/rGO composite was prepared by a relatively simple, scalable process, avoiding the need for expensive reagents and allowing for straightforward electrode modification.

Furthermore, while some sensors, such as PTTB/GCE[60] and MIP-PANI/GO/CPE,[61] showed detection limits of 0.05 μM and even as high as 20 μM, respectively, the latter demonstrates that not all reported sensors exceed our detection performance, especially in cost-effective designs. Our sensor offers adequate sensitivity for field-level screening and rapid diagnostics, with excellent repeatability and fabrication simplicity. Supporting this, the statistical model in Table 1 (ANOVA analysis) reveals that 4-NP concentration, scan rate, and their interaction (AB and AC) significantly affect current response ($p < 0.05$), confirming the reproducibility and statistical significance of the sensor's behavior. The model's high R^2 (0.9860) and adjusted R^2 (0.9681) indicate a strong correlation between experimental and predicted values, validating the robustness of the proposed sensor. While we acknowledge that further enhancement is needed to meet drinking water regulatory limits, this work serves as a foundational step toward developing scalable and efficient electrochemical platforms for environmental monitoring of toxic pollutants like 4-NP. The high R^2 value (0.9860) from the ANOVA analysis reflects the strong predictive capability of the developed regression model. Comparable studies have reported similarly high coefficients when evaluating nanocomposite-based electrochemical sensors for 4-NP. For instance, PEDOT:PSS-modified Pt NP-embedded PPy-CB@ZnO nanocomposites achieved an R^2 of 0.9917, indicating excellent model reliability and linear response behavior.[62] Likewise, a pyridine diketopyrrolopyrrole-functionalized graphene oxide sensor demonstrated a highly linear calibration curve with strong correlation between analyte concentration and current response.[63] These findings align closely with our results, confirming that the CoS-NR/rGO system exhibits similarly robust and well-fitted electrochemical performance.

Furthermore, the perturbation plot (Fig. 10b), which makes it easier to compare the effects of each element at a particular point in the design space, is used. The midpoint (coded 0) of every component served as the reference point. Nonetheless, the steep slope or curve of the component suggests that the reaction is sensitive to it, as illustrated for electrolyte pH and 4-NP concentration. While the scan rate is the minimal factor affecting the electrocatalytic activity of CoS-NR/rGO towards 4-NP.

4 Conclusions

In this study, a CoS-NR/rGO nanocomposite electrode was successfully fabricated using rGO derived from recycled plastic waste, combined with cobalt sulfide nanorods synthesized *via* a simple, low-cost chemical route employing thiourea and cobalt acetate. SEM and TEM analyses confirmed the well-defined morphology, while XRD, FTIR, Raman spectroscopy, and XPS verified the crystal structure and chemical composition essential for efficient electrochemical sensing. The CoS-NR/rGO electrode exhibited significantly enhanced performance for 4-NP detection compared to bare GCE and pure CoS-NR electrodes, with diffusion-controlled reduction, good selectivity, reusability, and long-term stability. The use of recycled rGO and straightforward synthesis steps markedly reduces material and processing costs relative to conventional sensors that rely on expensive noble metals or complex fabrication procedures. Coupled with its high surface area and simple assembly, the CoS-NR/rGO composite represents a cost-effective and practical platform for sensitive phenolic pollutant detection and environmental monitoring applications.

Conflicts of interest

There are no conflict to declare.

Data availability

Data will be available at request.

Acknowledgements

This work was supported and funded by the Deanship of Scientific Research at Imam Mohammad Ibn Saud Islamic Unversity (IMSIU) (grant number IMSIU-DDRSP2602).

References

1 M. Eriksen, L. C. M. Lebreton, H. S. Carson, M. Thiel, C. J. Moore, J. C. Borerro, F. Galgani, P. G. Ryan and J. Reisser, Plastic pollution in the world's oceans: More than 5 trillion plastic pieces weighing over 250,000 tons afloat at sea, *PLoS One*, 2014, **9**, e111913, DOI: 10.1371/journal.pone.0111913.

2 P. G. C. N. T. Pilapitiya and A. S. Ratnayake, The world of plastic waste: A review, *Clean. Mater.*, 2024, **11**, 100220, DOI: 10.1016/j.clema.2024.100220.

3 J. N. Hahladakis, C. A. Velis, R. Weber, E. Iacovidou and P. Purnell, An overview of chemical additives present in plastics: Migration, release, fate and environmental impact during their use, disposal and recycling, *J. Hazard. Mater.*, 2018, **344**, 179, DOI: 10.1016/j.jhazmat.2017.10.014.

4 N. Panigrahy, A. Priyadarshini, M. M. Sahoo, A. K. Verma, A. Daverey and N. K. Sahoo, A comprehensive review on eco-toxicity and biodegradation of phenolics: Recent progress and future outlook, *Environ. Technol. Innovat.*, 2022, **27**, 102423, DOI: 10.1016/j.eti.2022.102423.

5 H. Barakat, I. A. Alkabeer, T. Aljutaily, M. S. Almujaydil, R. M. Algheshairy, R. M. Alhomaid, A. S. Almutairi and A. Mohamed, Phenolics and Volatile Compounds of Fennel (Foeniculum vulgare) Seeds and Their Sprouts Prevent Oxidative DNA Damage and Ameliorates CCl4-Induced Hepatotoxicity and Oxidative Stress in Rat, *Antioxidants*, 2022, **1**, 2318, DOI: 10.3390/antiox11122318.

6 N. N. M. Zain, N. K. Abu Bakar, S. Mohamad and N. M. Saleh, Optimization of a greener method for removal of phenol

species by cloud point extraction and spectrophotometry, *Spectrochim. Acta, Part A*, 2014, **118**, 1121–1128, DOI: 10.1016/j.saa.2013.09.129.

7 A. A. Al-Kahtani, T. Almuqati, N. Alhokbany, T. Ahamad, M. Naushad and S. M. Alshehri, A clean approach for the reduction of hazardous 4-nitrophenol using gold nanoparticles decorated multiwalled carbon nanotubes, *J. Clean. Prod.*, 2018, **191**, 429–435, DOI: 10.1016/j.jclepro.2018.04.197.

8 A. M. Mostafa, E. A. Mwafy, A. M. Khalil, A. Toghan and E. A. Alashkar, ZnO/Ag multilayer for enhancing the catalytic activity against 4-nitrophenol, *J. Mater. Sci.: Mater. Electron.*, 2023, **34**, 300, DOI: 10.1007/s10854-022-09631-6.

9 F. S. Alamro, A. M. Mostafa, H. A. Ahmed and A. Toghan, Zinc oxide/carbon nanotubes nanocomposite: Synthesis, characterization and catalytic reduction of 4-nitrophenol via laser assistant method, *Surf. Interfaces*, 2021, **26**, 101406, DOI: 10.1016/j.surfin.2021.101406.

10 US EPA, *Quality Criteria for Water*, US Department of Commerce, National Technical Information Service, US Environmental Protection Agency, Springfield, Virginia, 1986, PB87-226759, EPA 440/5 86-001.

11 F. A. Harraz, M. A. Rashed, M. Faisal, M. Alsaiari and S. A. Alsareii, Sensitive and selective electrochemical sensor for detecting 4-nitrophenol using novel gold nanoparticles/reduced graphene oxide/activated carbon nanocomposite, *Colloids Surf. A Physicochem. Eng. Asp.*, 2022, **654**, 130068, DOI: 10.1016/j.colsurfa.2022.130068.

12 F. Dong, L. Chen, R. Wang, W. Yang, T. Lu and Y. Zhang, 4-Nitrophenol exposure in T24 human bladder cancer cells promotes proliferation, motilities, and epithelial-to-mesenchymal transition, *Environ. Mol. Mutagen.*, 2020, **61**, 316–328, DOI: 10.1002/em.22345.

13 H. F. Assaf, H. Salah, N. Hashem, M. Khodari and A. Toghan, Fabrication of an electrochemical sensor based on copper waste wire recycling and its application, *Sensor Actuator Phys.*, 2021, **331**, 112962, DOI: 10.1016/j.sna.2021.112962.

14 A. Toghan, M. Abd-Elsabour and A. M. Abo-Bakr, A novel electrochemical sensor based on EDTA-NQS/GC for simultaneous determination of heavy metals, *Sensor Actuator Phys.*, 2021, **322**, 112603, DOI: 10.1016/j.sna.2021.112603.

15 L. I. Trakhtenberg, Sensor layers based on semiconductor nanoparticles and their electronic structure, *Russ. J. Phys. Chem. B*, 2023, **17**, 600–607, DOI: 10.1134/S1990793123030144.

16 F. Wang and S. Hu, Electrochemical sensors based on metal and semiconductor nanoparticles, *Microchim. Acta*, 2009, **165**, 1–22, DOI: 10.1007/s00604-009-0136-4.

17 M. Vazan, J. Tashkhourian and B. Haghighi, A novel electrochemical sensor based on MoO_3 nanobelt–graphene oxide composite for the simultaneous determination of paracetamol and 4-aminophenol, *Diamond Relat. Mater.*, 2023, **140**(B), 110549, DOI: 10.1016/j.diamond.2023.110549.

18 X. Deng, L. Zhang, J. Guo, Q. Chen and J. Ma, ZnO enhanced NiO-based gas sensors towards ethanol, *Mater. Res. Bull.*, 2017, **90**, 170–176, DOI: 10.1016/j.materresbull.2017.02.040.

19 Y. Gao, W. Zhou, D. Kong, J. Han, Y. Gao and G. Lu, Moisture-independent detection of n-propanol using a kinetic gas sensor based on CdS nanorods coated with reduced graphene oxide, *ACS Appl. Nano Mater.*, 2023, **6**, 19588–19598, DOI: 10.1021/acsanm.3c02674.

20 A. Toghan, N. Roushdy, S. A. Al-Hussain, M. S. Elnouby, S. M. Yousef, A. A. M. Farag, M. E. Youssef and N. A. Elessawy, Assessing the performance of novel and sustainable electrochemical sensor based on cobalt sulfide/upcycled reduced graphene oxide from plastic waste, *Electrochem. Commun.*, 2025, **177**, 107982, DOI: 10.1016/j.elecom.2025.107982.

21 A. K. Geim and K. S. Novoselov, The rise of graphene, *Nanoscience and Technology: A Collection of Reviews from Nature Journals*, 2009, 652, 11–19. DOI: 10.1142/9789814287005_0002.

22 J. Wu, W. Pisula and K. Müllen, Graphenes as potential material for electronics, *Chem. Rev.*, 2007, **107**, 718–747, DOI: 10.1021/cr068010r.

23 N. Veeramani, D. R. Kumar, N. T. Manikandanath, A. Sri Ganesh, G. Siju and G. Srinivas, Investigation of microcapsules-based self-healing composites embedded with carbon nanotubes for improved healing efficiency, *J. Polym. Res.*, 2024, **31**, 312, DOI: 10.1007/s10965-024-04155-5.

24 P. Xu, T. Erdem and E. Eiser, A simple approach to prepare self-assembled, nacre-inspired clay/polymer nanocomposites, *Soft Matter*, 2020, **16**, 5402–5413, DOI: 10.1039/D0SM00476B.

25 V. Naveen, A. P. Deshpande and S. Rajaa, Self-healing microcapsules encapsulated with carbon nanotubes for improved thermal and electrical properties, *RSC Adv.*, 2020, **10**, 33178–33188, DOI: 10.1039/D0RA06631A.

26 N. Toyama, H. Kimura, N. Matsumoto, S. Kamei, D. N. Futaba, N. Terui and S. Furukawa, Enhanced activity for reduction of 4-nitrophenol of Ni/single-walled carbon nanotube prepared by super-growth method, *Nanotechnology*, 2022, **33**, 065707, DOI: 10.1088/1361-6528/ac353f.

27 N. Veeramani, M. Devine, J. A. Quinn, A. K. Alapati, A. Bolluk and D. Ray, Enhancing fracture toughness of carbon fiber/epoxy composites using polyphenylene ether as a modifier, *J. Appl. Polym. Sci.*, 2024, **141**, e55388, DOI: 10.1002/app.55388.

28 N. A. Elessawy, M. H. Gouda, M. F. Elkady, S. M. Ali, M. Gouda and M. S. Mohy Eldin, Ultra-fast removal of cadmium and lead from wastewater using high-efficient adsorbent derived from plastic waste: Statistical modeling, kinetic and isotherm studies, *Desalination Water Treat.*, 2020, **173**, 394–408, DOI: 10.5004/dwt.2020.24809.

29 N. A. Elessawy, M. H. Gouda, S. M. Ali, M. Salerno and M. S. Mohy Eldin, Effective elimination of contaminant antibiotics using high-surface-area magnetic-functionalized graphene nanocomposites developed from plastic waste, *Materials*, 2020, **13**, 1517, DOI: 10.3390/ma13071517.

30 J. Zhou, A. Cunha and M. N. Do, Nonsubsampled contourlet transform: Construction and application in enhancement, *Proceedings of IEEE International Conference on Image*

Processing, ICIP, 2004, 1, 469–472, DOI: 10.1109/ICIP.2005.1529789.

31 P. Hyerim, B. Dasol, P. No-Kuk, K. Minkyu and K. Misook, Self-assembled CoS/S-rGO dual-functional composite, and reliable hydrogen evolution performance in both acidic and alkaline media, *Mater. Today Adv.*, 2023, **19**, 100404, DOI: 10.1016/j.mtadv.2023.100404.

32 N. Chadha, R. Sharma and P. Saini, A new insight into the structural modulation of graphene oxide upon chemical reduction probed by Raman spectroscopy and X-ray diffraction, *Carbon Lett.*, 2021, **31**, 1125–1131, DOI: 10.1007/s42823-021-00234-5.

33 T. Xu, Z. Wang, G. Wang, L. Lu, S. Liu, S. Gao, H. Xu and Z. Yu, One-pot synthesis of a CoS-AC electrode in a redox electrolyte for high-performance supercapacitors, *J. Appl. Electrochem.*, 2019, **49**, 1069–1077, DOI: 10.1007/s10800-019-01341-y.

34 N. A. Elessawy, J. Exley, D. S. El-Sayed, A. Toghan, S. A. Al-Hussain, M. Elzokm, A. H. Konsowa and M. Tillotson, Development of an efficient, low-operating-pressure graphene oxide/polyethersulfone nanofiltration membrane for removing various water contaminants, *J. Environ. Chem. Eng.*, 2024, **12**, 112489, DOI: 10.1016/j.jece.2024.112489.

35 L. Yin, L. Wang, X. Liu, Y. Gai, L. Su, B. Qu and L. Gong, Ultra-fast microwave synthesis of 3D flower-like Co_9S_8 hierarchical architectures for high-performance supercapacitor applications, *Eur. J. Inorg. Chem.*, 2015, **14**, 2457–2462, DOI: 10.1002/ejic.201500120.

36 J. Li, F. Luo, Q. Zhao, W. Liu and D. Xiao, Low-temperature coprecipitation synthesis of amorphous nickel cobalt sulfide nanoparticles for high-performance supercapacitors, *J. Mater. Sci.: Mater. Electron.*, 2019, **30**, 14538–14546, DOI: 10.1007/s10854-019-01825-9.

37 Y. Zuo, W. Zhang, J. Che, S. Feng, Y. Chen and C. Wang, Efficient extraction of cobalt and copper: Leveraging redox chemistry in oxide and sulfide copper-cobalt ores, *Sep. Purif. Technol.*, 2025, **354**, 128671, DOI: 10.1016/j.seppur.2024.128671.

38 A. Dhamodharan, E. Murugan, H. Li, X. Zheng, Y. Gao, T. Guan, S. Rao, H. Pang and K. Perumal, Hexagonal morphology nickel sulfide anchored on graphene oxide–modified glassy carbon electrode for the sensitive detection of paracetamol in biological samples, *Electrocatalysis*, 2025, **16**, 182–195, DOI: 10.1007/s12678-024-00909-3.

39 J. Yuan, L. Jiang, J. Che, G. He and H. Chen, Composites of NiS_2 microblocks, MoS_2 nanosheets, and reduced graphene oxide for energy storage and electrochemical detection of bisphenol A, *ACS Appl. Nano Mater.*, 2021, **4**, 6093–6102, DOI: 10.1021/acsanm.1c00908.

40 M. K. Alam, M. M. Rahman, M. Abbas, S. R. Torati, A. M. Asiri, D. Kim and C. G. Kim, Ultra-sensitive 2-nitrophenol detection based on reduced graphene oxide/ZnO nanocomposites, *J. Electroanal. Chem.*, 2017, **788**, 66–73, DOI: 10.1016/j.jelechem.2017.02.004.

41 R. Su, H. Tang and F. Xi, Sensitive electrochemical detection of p-nitrophenol by pre-activated glassy carbon electrode integrated with silica nanochannel array film, *Front. Chem.*, 2022, **10**, 954748, DOI: 10.3389/fchem.2022.954748.

42 Y. Zhang, Y. Wang, W. Meng, J. Zhang, Y. Wang, B. Tong and C. Han, One stone, three birds: The enhanced electrocatalytic sensing for 4-nitrophenol derived from the triple-strategies regulated interface of Co-ZIF-L/NCS/CP, *Sens. Actuators, B*, 2025, **422**, 136682, DOI: 10.1016/j.snb.2024.136682.

43 N. L. N. Trang, D. T. N. Nga, V.-T. Hoang, X.-D. Ngo, P. T. Nhung and A.-T. Le, Bio-AgNPs-based electrochemical nanosensors for the sensitive determination of 4-nitrophenol in tomato samples: the roles of natural plant extracts in physicochemical parameters and sensing performance, *RSC Adv.*, 2022, **12**, 6007–6017, DOI: 10.1039/D1RA09202B.

44 Y. Qiao, J. Li, Y. Sun and Q. Li, Application of Bismuth Film/Nichrome Electrode for electrocatalytic reduction of 4-nitrophenol, *Asian J. Chem.*, 2014, **26**, 7949–7953, DOI: 10.14233/ajchem.2014.16777.

45 F. Zhou, J. Wang, Y. Tang, X. Song, W. Zhou, Y. Li and F. Gao, Enhanced sensing performance of flexible non-enzymatic electrochemical glucose sensors using hollow Fe_3O_4 nanospheres of controllable morphologies, *Ceram. Int.*, 2024, **50**, 38009–38021, DOI: 10.1016/j.ceramint.2024.07.162.

46 Z. Wu, X. Du and J. Zhang, Fabrication of a novel electrochemical sensing platform for voltammetric screening of prednisolone as a doping agent in sport, *Alex. Eng. J.*, 2024, **96**, 93–98, DOI: 10.1016/j.aej.2024.03.098.

47 N. A. Elessawy, A. G. Alhamzani, S. A. J. Almahmoud and B. S. Hsiao, Evaluation, optimization study, and life cycle assessment of novel eco-friendly PVA-based nanocomposite hydrogel adsorbents for methylene blue and paracetamol removal, *Ecotoxicol. Environ. Saf.*, 2024, **285**, 117123, DOI: 10.1016/j.ecoenv.2024.117123.

48 P. Deng, Z. Xu, Y. Feng and J. Li, Electrocatalytic reduction and determination of p-nitrophenol on acetylene black paste electrode coated with salicylaldehyde-modified chitosan, *Sens. Actuators, B*, 2012, **168**, 381–389, DOI: 10.1016/j.snb.2012.04.041.

49 L. Q. Luo, X. L. Zou, Y. P. Ding and Q. S. Wu, Derivative voltammetric direct simultaneous determination of nitrophenol isomers at a carbon nanotube modified electrode, *Sens. Actuators, B*, 2008, **135**, 61–65, DOI: 10.1016/j.snb.2008.07.019.

50 S. Hu, C. Xu, G. Wang and D. Cui, Voltammetric determination of 4-nitrophenol at a sodium montmorillonite–anthraquinone chemically modified glassy carbon electrode, *Talanta*, 2001, **54**, 115–123, DOI: 10.1016/S0039-9140(00)00658-5.

51 S. A. Hira, J. Quintal and A. Chen, Sensitive electrochemical determination of vanillin using a bimetallic hydroxide and reduced graphene oxide nanocomposite, *Sensors*, 2025, **25**, 1694, DOI: 10.3390/s25061694.

52 C. Karuppiah, S. Palanisamy, S. Chen, R. Emmanuel, M. A. Ali, P. Muthukrishnan, P. Prakash and F. M. A. Hemaid, Electrochemical detection of 4-

nitrophenol based on biomass derived activated carbons, *J. Solid State Electrochem.*, 2014, **18**, 1847–1854, DOI: 10.1007/s10008-014-2381-4.

53 Z. Wang, A. He and L. Liu, Electrochemical study and synthesis of highly ordered TiO_2 nanorod arrays on 3D graphene oxide framework as photocatalyst for Acid Orange 7 degradation, *Int. J. Electrochem. Sci.*, 2022, **17**, 220645, DOI: 10.20964/2022.06.46.

54 N. Baydogan, O. Karacasu and H. Cimenoglu, Effect of annealing temperature on ZnO:Al/p-Si heterojunctions, *Thin Solid Films*, 2012, **520**, 5790–5796, DOI: 10.1016/j.tsf.2012.04.044.

55 X. Zhang, Z. Lai, C. Tan and H. Zhang, Solution-processed two-dimensional MoS_2 nanosheets: Preparation, hybridization, and applications, *Angew. Chem., Int. Ed.*, 2016, **55**, 8351–8356, DOI: 10.1002/anie.201509933.

56 M. Faisal, M. M. Alam, M. Alsaiari, J. Ahmed, J. Y. Al-Humaidi, J. S. Algethami, M. A. Abdel-Fadeel, R. H. Althomali, F. A. Harraz and M. M. Rahman, Efficient 2-nitrophenol determination based on ultrasonochemically prepared low-dimensional Au-nanoparticles decorated ZnO–chitosan nanocomposites by linear sweep voltammetry, *J. Sci. Adv. Mater. Devices*, 2024, **9**, 100727, DOI: 10.1016/j.jsamd.2024.100727.

57 C. Yin, Y. Liu, T. Hu and X. Chen, Graphitic carbon nitride nanomaterials-based electrochemical sensing interfaces for monitoring heavy metal ions in aqueous environments, *Nanomaterials*, 2025, **15**, 564, DOI: 10.3390/nano15070564.

58 X. Han, Development of electrochemical immunosensor for detecting salbutamol by competitive immune strategy, *Int. J. Electrochem. Sci.*, 2020, **15**, 7337–7346, DOI: 10.20964/2020.08.93.

59 I. Shakir and M. Sarfraz, Evaluation of electrochemical charge storage mechanism and structural changes in intertwined MoO_3–MWCNTs composites for supercapacitor applications, *Electrochim. Acta*, 2014, **147**, 380–384, DOI: 10.1016/j.electacta.2014.09.

60 D. Chen, Y. Cheng, N. Zhou, P. Chen, Y. Wang, K. Li, S. Huo, P. Cheng, P. Peng, R. Zhang, L. Wang, H. Liu, Y. Liu and R. Ruan, Photocatalytic degradation of organic pollutants using TiO_2-based photocatalysts: A review, *J. Clean. Prod.*, 2020, **268**, 121725, DOI: 10.1016/j.jclepro.2020.121725.

61 T. Kunitake, Polyion complexation in solution, at interface and on surface: Legacy for layer-by-layer assembly, *J. Taiwan Inst. Chem. Eng.*, 2018, **92**, 15–19, DOI: 10.1016/j.jtice.2018.02.008.

62 M. Faisal, M. M. Alam, J. Ahmed, A. M. Asiri, M. Jalalah, R. S. Alruwais, M. M. Rahman and F. A. Harraz, Sensitive electrochemical detection of 4-nitrophenol with PEDOT:PSS modified Pt NPs-embedded PPy-CB@ZnO nanocomposites, *Biosensors*, 2022, **12**, 990, DOI: 10.3390/bios12110990.

63 L. Jia, J. Hao, S. Wang, L. Yang and K. Liu, Sensitive detection of 4-nitrophenol based on pyridine diketopyrrolopyrrole-functionalized graphene oxide direct electrochemical sensor, *RSC Adv.*, 2023, **13**, 2392–2401, DOI: 10.1039/D2RA07239D.